Progress In Electromagnetics Research Letters, Vol. 83, 37–44, 2019

A Method of Reducing Air-Gap Harmonic of Permanent Magnet Motor for Fitness Car

Jiancheng Zang[1], Yan Wang[1], and Libing Jing[2, *]

Abstract—In order to solve the high harmonic content of permanent magnet synchronous motor (PMSM) for fitness car, a PMSM with built-in permanent magnet bridge is proposed in this paper. Compared with surface mounted permanent magnet synchronous motor (SM-PMSM), the proposed motor with permanent magnet bridge structure has lower harmonic content. The performance and magnetization angle of the proposed motor are compared and analyzed in detail. The results obtained from finite element analysis show that the permanent magnet bridge can increase the air gap magnetic field intensity, and different directions of magnetization will affect the amplitude of fundamental wave of air gap magnetic density. Moreover, it can reduce the total harmonic distortion (THD) and make the magnetic density waveform more sinusoidal. It is very beneficial to the smooth output of torque of fitness car.

1. INTRODUCTION

With the development of magnetic materials and the progress of motor control technology, permanent magnet synchronous motor (PMSM) has become one of the research hotspots in the field of motor. PMSM can be divided into three types according to its permanent magnet assembling mode: surface mounted type, interior type and hybrid type (surface mounted-interior type). PMSM has excellent electromagnetic performance, but the application of PMSM is limited due to excessive internal harmonics. In this regard, how to suppress harmonics is the key to the design of permanent magnet synchronous motor [1–4]. Many literatures about surface mounted permanent magnet synchronous motor and interior permanent magnet synchronous motor have done extensive research [5–9], and the research potential of hybrid permanent magnet synchronous motor is great.

At present, there are three main solutions for air gap flux density optimization of permanent magnet synchronous motors: 1) optimizing the shape of permanent magnets (PM) [10, 11]; 2) accurately controlling the magnetization process [12, 13]; 3) adopting a new structure of permanent magnet motors [14, 15]. In [16], an improved analytical method for calculating the magnetic field and cogging torque of surface mounted PMSM with arbitrary eccentric rotor shape is proposed, which can greatly reduce the harmonic content of radial flux density. Reference [17] presents a new shape optimization method for permanent magnets based on the magnetic field distribution of nonuniform permanent magnets, which is used for reducing the harmonic and iron loss of magnetic field. In [18], two IPM rotor topologies in electric vehicles have been designed and analyzed, and it is concluded that dual-U shape has good torque performance, superior controllability performance, and small mechanical stress. It is recommended that dual-U shape is suitable for the rotor topology in the power and speed range. In [19], a new method namely T-shaped bifurcation in stator teeth to reduce the cogging torque in radial flux surface mounted Permanent Magnet Brushless DC (PMBLDC) motor has been proposed.

Received 22 January 2019, Accepted 19 March 2019, Scheduled 27 March 2019

* Corresponding author: Libing Jing (jinglibing163@163.com).

[1] College of Physical Education, China Three Gorges University, Yichang 443002, China. [2] College of Electrical Engineering & New Energy, China Three Gorges University, Yichang 443002, China.

The proposed method has been designed using CAD package *MagNet* software. From the performance results, the proposed T-shaped bifurcation yields much reduced cogging torque as compared to existing and bifurcation techniques in stator slots.

In this paper, on the basis of surface mounted magnetic poles, a permanent magnet bridge is constructed between magnetic poles to reduce magnetic leakage, increase the air gap magnetic density, reduce the air gap harmonics, and improve the sinusoidal ratio of the air gap waveform. A schematic diagram of the motor structure is shown in Fig. 1.

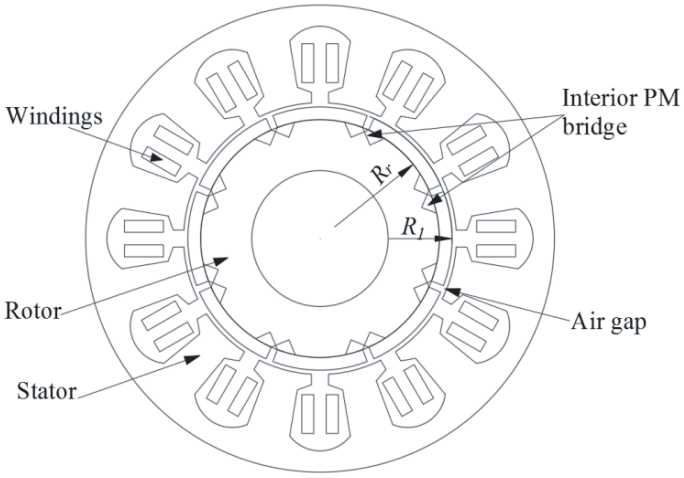

Figure 1. PMSM with interior PM bridge.

2. INTERIOR PM BRIDGE STRUCTURE

Figure 2 shows the schematic diagram of the interior PM bridge. The interior PM bridge can be divided into two categories: Fig. 2(a) shows the interior right angle PM bridge, and Fig. 2(b) is the interior arc PM bridge. The former part of the interior PM bridge is placed at right angle, while the latter part of the interior PM bridge is placed at arc.

In Fig. 2, pole distance is expressed by W_p, and magnetic pole arc is expressed by W_f. Therefore, the pole arc coefficient α_p can be expressed as

$$\alpha_p = \frac{W_f}{W_p} \tag{1}$$

Surface-mounted poles are radial magnetized; h_m is the thickness of the interior PM bridge; a and b are the upper and lower lengths of the interior PM bridge, respectively. The volume of PM at each pole can be expressed as the sum of surface mounted PM and interior PM bridge. The volume of surface mounted PM at one pole is,

$$V_1 = \frac{W_f \pi (R_1^2 - R_r^2)}{360^\circ} * D \tag{2}$$

where R_1 and R_r are the radius of PM and the outer radius of rotor respectively. D is the effective axis length of the motor.

In the right angle PM bridge, the volume of PM bridge at one pole is,

$$V_2 = (a + b) * h_m * D \tag{3}$$

where h_m is the height of PM bridge.

In the arc PM bridge, the volume of PM bridge at one pole is,

$$V_3 = \frac{1}{2}\alpha * h_m^2 * D \tag{4}$$

where α is the angle between two bridges.

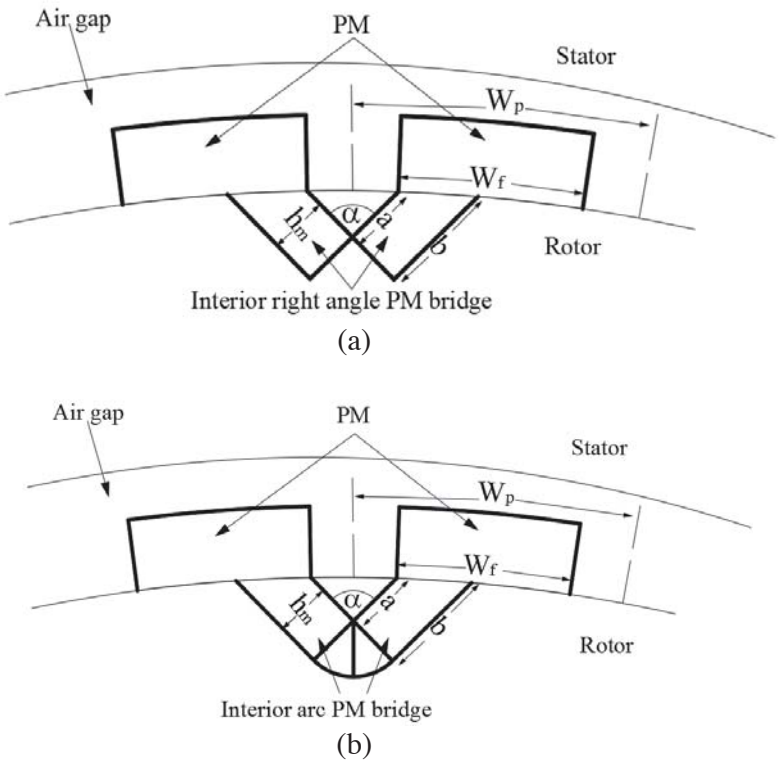

Figure 2. Schematic diagram of the interior PM bridge. (a) Right angle PM bridge. (b) Arc PM bridge.

3. FINITE ELEMENT ANALYSIS CALCULATION

In order to verify the accuracy of the proposed method, an 8-pole 12-slot surface mounted-interior PM bridge synchronous motor is used as an example to simulate. The main parameters of the motor are shown in Table 1.

Figure 3 shows the distribution of the magnetic lines of the three structural models. It can be seen from the figures that the magnetic density of the improved model is higher than that of the tabular model.

Figure 4 shows the radial magnetic density amplitude of the air gap obtained by Fast Fourier Transform.

As can be seen from Fig. 4, the conventional surface mounted PMSM has high harmonic content, especially 12th and 28th order harmonics in the air gap. However, after optimization and improvement, the interior PM bridge structure motor enlarges the fundamental wave amplitude and reduces the high-order harmonics. The waveform of the built-in arc permanent magnet bridge is closer to sinusoidal, and the fundamental wave amplitude is the largest.

In order to further analyze the harmonics of air gap magnetic density, the total harmonic distortion (THD) of air gap magnetic field is introduced to measure the sinusoidal waveform of air gap magnetic density in different structures.

$$\mathrm{THD} = \frac{\sqrt{\sum_{k=2}^{\infty} B_k^2}}{B_1} \times 100\% \tag{5}$$

where B_1 is the fundamental wave amplitude, and B_k is the Kth harmonic amplitude.

The THD of three structures can be calculated by formula (5), Table 2 is the result of THD calculation.

Table 1. Main parameters of motor structure.

Parameter	value
Pole pairs	4
Number of slots	12
Inner radius of rotor/mm	32
Outer radius of rotor/mm	56
Inner radius of stator/mm	64
Outer radius of stator/mm	110
Length of PM/mm	7
Height of PM bridge/mm	1
Air gap length/mm	1
Lower length of PM bridge/mm	2
Upper length of PM bridge/mm	1
Rated speed/r/min	100
Remanence/T	1.1
Axial length/mm	65

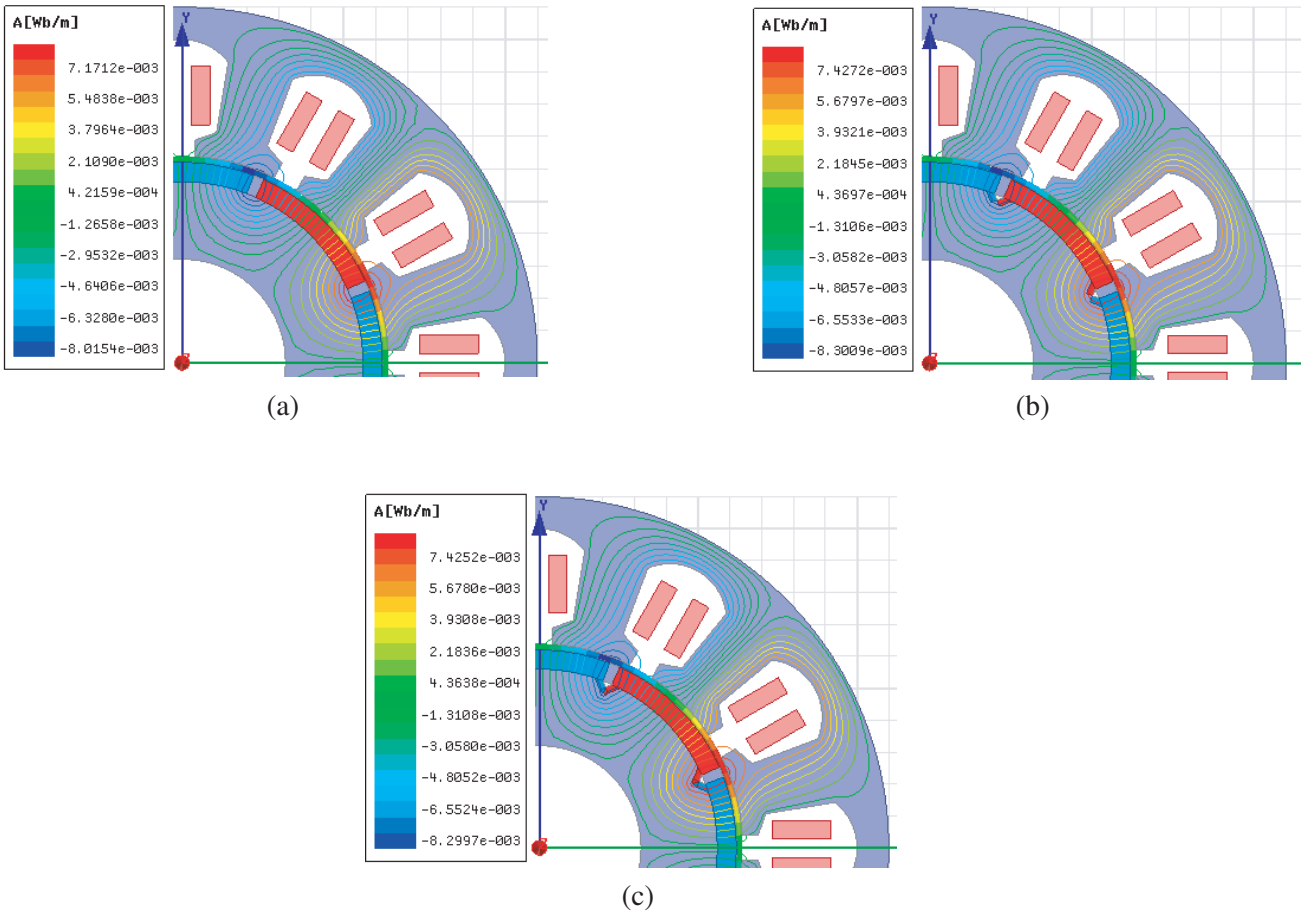

Figure 3. Magnetic field distribution. (a) Conventional model. (b) Right angle PM bridge. (c) Arc PM bridge.

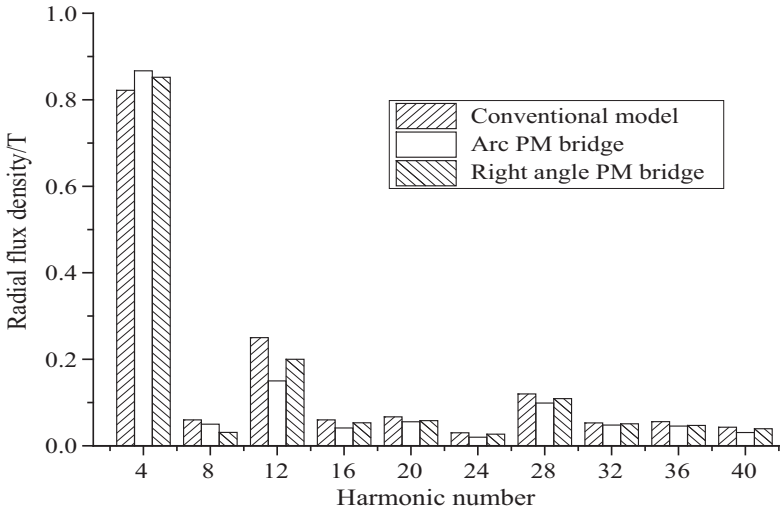

Figure 4. Harmonic spectra of radial flux density in the air-gaps.

Table 2. THD of different structures.

Structures	THD (%)
Conventional	37.94
Right angle PM bridge	24.55
Arc PM bridge	30.19

4. INFLUENCE OF MAGNETIC FLUX DIRECTION ON HARMONICS OF PM BRIDGE

Surface-mounted PMs are magnetized radially, and the direction of magnetization of the interior PM bridge is $\Delta\theta$ degree with the radial direction. The specific direction of magnetization is shown in Fig. 5.

In order to reduce the harmonic content of air gap, $\Delta\theta$ is magnetized at different angles and simulated. The air-gap magnetic density is considered in terms of $\Delta\theta$ = 30°, 45°, 60°, and 90°,

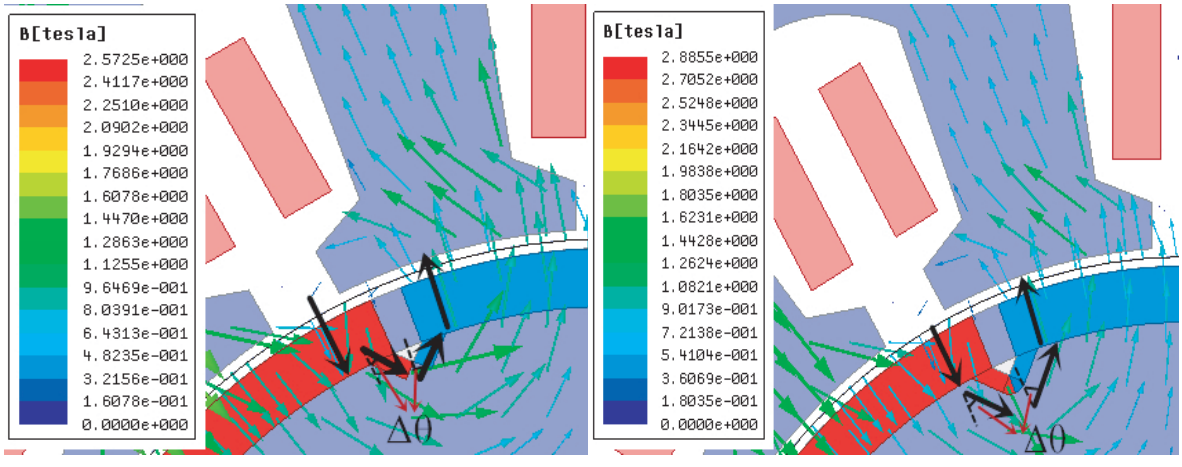

(a) (b)

Figure 5. Two ways of magnetization. (a) Right angle PM bridge. (b) Arc PM bridge.

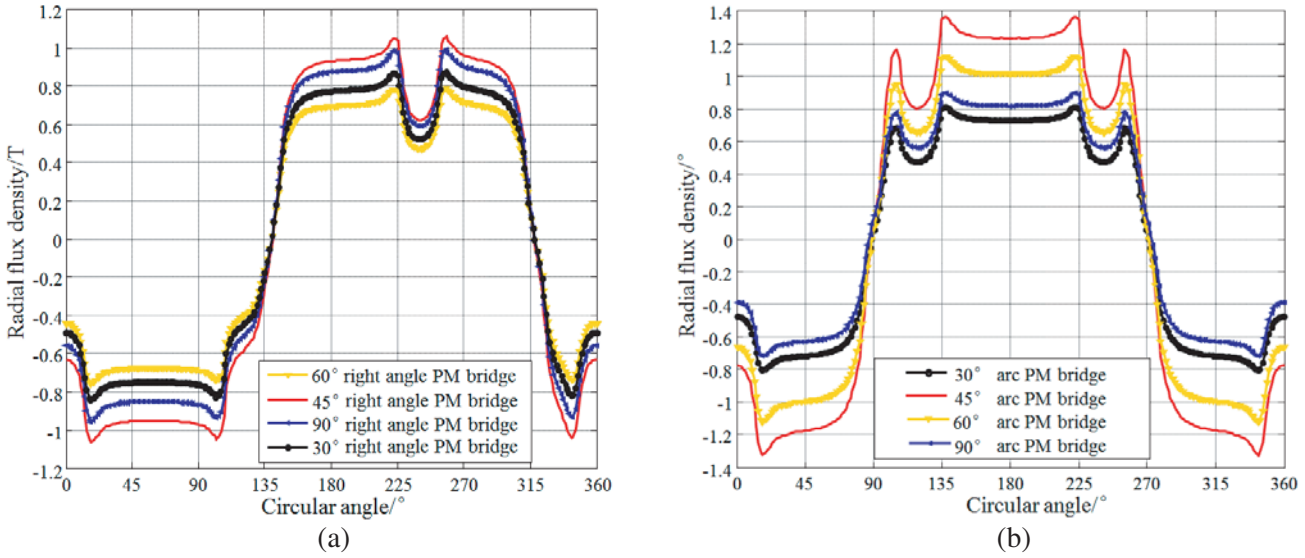

Figure 6. Flux density distribution at different angles. (a) Right angle PM bridge. (b) Arc PM bridge.

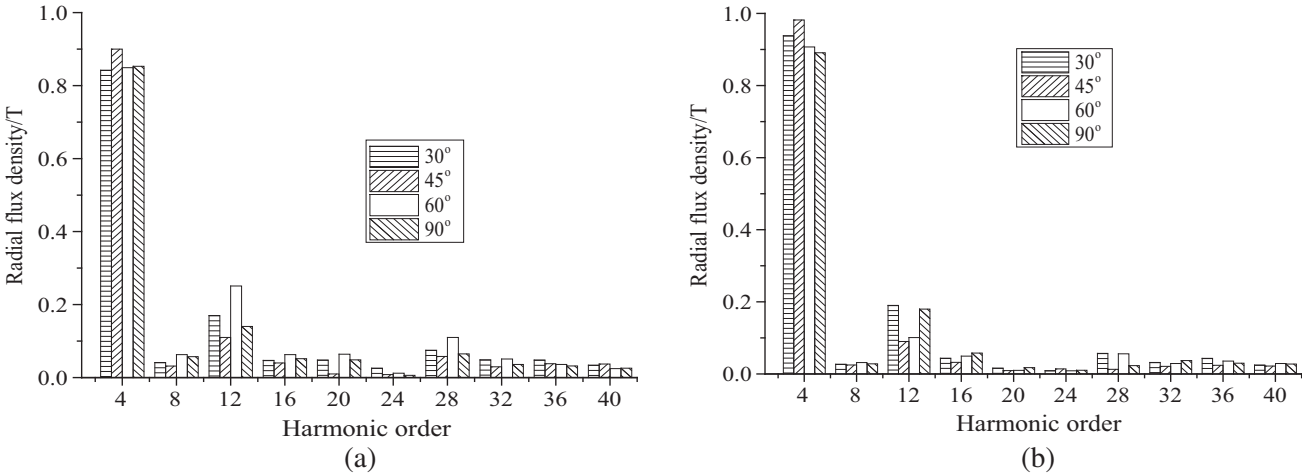

Figure 7. Harmonic spectra of radial flux density. (a) Right angle PM bridge. (b) Arc PM bridge.

respectively. Fig. 6 shows the radial flux density waveforms of air gap under two different configurations. Fig. 7 shows the radial magnetic density amplitude of the air gap obtained by Fast Fourier Transform. The corresponding THD is listed in Table 3.

It can be seen from Fig. 7 that the maximum fundamental wave is 45°, and the minimum fundamental wave is 30° in the magnetization angle of the interior right angle PM bridge. Among them, the 8th, 12th, and 28th harmonics are high. At the same time, in the magnetization angle of the interior arc PM bridge, the maximum fundamental wave is 45°, and the minimum fundamental wave is 9°. Among them, the 12th, 16th, and 28th harmonics are high.

As can be seen from Fig. 7 and Table 3, compared with the surface mounted PM motor structure, the interior arc PM bridge has smaller harmonics and smaller THD than the interior right angle PM bridge in the same angle. However, when $\Delta\theta = 90°$, the THD of the interior right angle PM bridge is smaller than interior arc PM bridge. It can be seen that the THD of the same structure is small at 45° magnetization angle. In summary, the interior arc PM bridge has the largest fundamental wave, the smallest harmonic and the THD at 45° magnetization angle.

Table 3. The effect of $\Delta\theta$ on THD.

$\Delta\theta/(^\circ)$	THD (%)	
	Right angle PM bridge	Arc PM bridge
30	25.81%	22.82%
45	16.45%	11.02%
60	35.68%	15.55%
90	21.99%	22.58%

5. CONCLUSION

A novel surface mounted PMSM with interior PM bridge is proposed in this paper. Through the finite element simulation analysis of different structures and different angles of magnetization under the same angle of magnetization, it can be found that the proposed interior arc PM bridge structure motor can increase the fundamental wave amplitude of air gap magnetic density, reduce high-order harmonics, and magnetic flux density waveform of air gap is more sinusoidal. The THD is smaller, and the value is 11.02%. It can be used for fitness car to improve the efficiency of PMSM operation and reduce the torque ripple of the motor.

ACKNOWLEDGMENT

This work was supported by the National Natural Science Foundation of China (Project No: 51707072), China Postdoctoral Science Foundation (Project No: 2018M632855).

REFERENCES

1. Li, L., K. M. Lee, K. Bai, X. P. Ouyang, and H. Y. Yang, "Inverse models and harmonics compensation for suppressing torque ripples of multiphase permanent magnet motor," *IEEE Trans. Ind. Electro.*, Vol. 65, No. 11, 8730–8739, Feb. 2018.
2. Kumar, D. and K. Chaudhary, "Design of differential source fed circularly polarized rectenna with embedded slots for harmonics suppression," *Progress In Electromagnetics Research C*, Vol. 84, 175–187, 2018.
3. Jin, X. H., B. S. Li, and D. G. Xu, "A current harmonics suppression method for permanent magnet synchronous motor drives," *2017 IEEE Transportation Electrification Conference and Expo, Asia-Pacific (ITEC Asia-Pacific)*, 1–6, 2017.
4. Azeez, N. A., K. Gopakumar, J. Mathew, and C. Cecati, "A harmonic suppression scheme for open-end winding split-phase IM drive using capacitive filters for the full speed range," *IEEE Trans. Ind. Electro.*, Vol. 61, No. 1, 5213–5221, Feb. 2014.
5. Tiang, T. L., D. Ishak, C. P. Lim, and M. K. Jamil, "A comprehensive analytical subdomain model and its field solutions for surface-mounted permanent magnet machines," *IEEE Trans. Magn.*, Vol. 51, No. 4, ID: 8104314, 2015.
6. Xie, K. F., D. W. Li, R. H. Qu, and D. Jiang, "Analysis and experimental comparison of spoke type and surfacemounted PM machines with fractional slot concentrated winding," *2016 19th International Conference on Electrical Machines and Systems (ICEMS)*, 1–6, 2016.
7. Hadef, M., M. R. Mekideche, A. Djerdir, and A. Miraoui, "An inverse problem approach for parameter estimation of interior permanent magnet synchronous motor," *Progress In Electromagnetics Research B*, Vol. 31, 15–28, 2011.
8. Zhao, N. N. and W. G. Liu, "Loss calculation and thermal analysis of surface-mounted PM motor and interior PM motor," *IEEE Trans. Magn.*, Vol. 51, No. 11, ID: 8112604, 2015.

9. Butt, C. B. and M. A. Rahman, "Untrained artificial neuron-based speed control of interior permanent-magnet motor drives over extended operating speed range," *IEEE Trans. Ind. Appl.*, Vol. 49, No. 3, 1146–1153, Mar. 2013.
10. Brahim, L.-C., K. Boughrara, and R. Ibtiouen, "Cogging torque minimization of surface-mounted permanent magnet synchronous machines using hybrid magnet shapes," *Progress In Electromagnetics Research B*, Vol. 62, 49–61, 2015.
11. Chen, Z. F., C. L. Xia, Q. Geng, and Y. Yan, "Modeling and analyzing of surface-mounted permanent magnet synchronous machines with optimized magnetic pole shape," *IEEE Trans. Magn.*, Vol. 5, No. 11, ID: 8102804, 2014.
12. Kim, K. S., M. R. Park, H. J. Kim, S. H. Chai, and J. P. Hong, "Estimation of rotor type using ferrite magnet considering the magnetization process," *IEEE Trans. Magn.*, Vol. 52, No. 3, ID: 811804, 2016.
13. Jiang, Y. D., R. Pei, W. Xian, and Z. Hong, "Magnetization process of an HTS motor and the torque ripple suppression," *IEEE Trans. Appl. Supercond.*, Vol. 19, No. 3, 1644–1647, 2009.
14. Tiang, T. L., D. Ishak, C. P. Lim, and M. Rezal Mohamed, "Analytical method using virtual PM blocks to represent magnet segmentations in surface-mounted PM synchronous machines," *Progress In Electromagnetics Research B*, Vol. 76, 23–36, 2017.
15. Onsal, M., B. Cumhur, Y. Demir, E. Yolacan, and M. Aydin, "Rotor design optimization of a new flux assisted consequent pole spoke-type permanent magnet torque motor for low-speed applications," *IEEE Trans. Magn.*, Vol. 54, No. 11, ID: 8206005, 2018.
16. Zhou, Y., H. Li, and G. Meng, "Analytical calculation of magnetic field and cogging torque in surface-mounted permanent-magnet machines accounting for any eccentric rotor shape," *IEEE Trans. Ind. Electro.*, Vol. 62, No. 6, 3438–3447, 2015.
17. Chai, F., P. Liang, and Y. Pei, "Magnet shape optimization of surface-mounted permanent-magnet motors to reduce harmonic iron losses," *IEEE Trans. Magn.*, Vol. 52, No. 7, ID: 6301304, 2016.
18. Zhang, X. J., L. B. Zeng, and R. L. Pei, "Designing and comparison of permanent magnet synchronous reluctance motors and conventional motors in electric vehicles," *2018 21st International Conference on Electrical Machines and Systems (ICEMS)*, 202–205, 2018.
19. Noyal Doss, A., R. Brindha, K. Mohanraj, S. S. Dash, and K. M. Kavya, "A novel method for cogging torque reduction in permanent magnet brushless DC motor using T-shaped bifurcation in stator teeth," *Progress In Electromagnetics Research M*, Vol. 66, 99–107, 2018.